Critical Crystallization for Embrittlement in Metallic Glasses

Jittisa Ketkaew,[1] Ze Liu,[1,2,*] Wen Chen,[1] and Jan Schroers[1,†]
[1]Department of Mechanical Engineering & Materials Science, Yale University, New Haven, Connecticut 06511, USA
[2]Department of Engineering Mechanics, School of Civil Engineering, Wuhan University, Wuhan 430072, China
(Received 13 September 2015; published 22 December 2015)

We studied the effect of crystallization on the embrittlement of bulk metallic glasses. Specifically, we measured fracture toughness for $Zr_{44}Ti_{11}Cu_{10}Ni_{10}Be_{25}$ and $Pd_{43}Cu_{27}Ni_{10}P_{20}$ after annealing at various times to introduce controlled volume fraction of crystallization. We found that crystallization of up to ~6% by volume does not measurably affect fracture toughness. When exceeding ~6%, a dramatic drop in fracture toughness occurs; an additional 1% of crystallization reduces fracture toughness by 50%. Such a dramatic transition can be explained by the interaction among the crystals' stress fields in the amorphous matrix that becomes effective at ~7% crystallinity. Our findings of a critical crystallization for embrittlement of metallic glasses help in designing tough metallic glasses and their composites, as well as defining processing protocols for the unique thermoplastic forming of metallic glasses to avoid embrittlement.

DOI: 10.1103/PhysRevLett.115.265502 PACS numbers: 62.20.F-, 62.20.mj, 81.40.Gh, 81.40.Lm

Within the material class of bulk metallic glasses (BMGs), fracture toughness varies from ideally brittle behavior such as that observed in magnesium-based BMG [1] to exceptionally tough, as observed in zirconium-based and precious metal BMGs [2–5]. Generally, measuring fracture toughness has been difficult for BMGs, reflected by the wide scatter in the fracture toughness values that have been reported for the same BMG [6]. Uncontrolled partial crystallization has been suggested as one origin for the observed wide scattering [6,7]. Because of the metastable nature of BMGs, crystallization can occur during liquid cooling or thermoplastic forming (TPF), and complete avoidance has proven difficult [8–11]. For the majority of BMG forming alloys, partial crystallization has been shown to degrade properties [12–17]. However, it has also been reported that in some cases, partial crystallization enhances fracture toughness [3,14,18,19]. To date, a quantitative understanding of the effect of partial crystallization of metallic glass forming alloys on their fracture toughness and, hence, a mechanistic understanding, is lacking.

Here, we study the effect of the crystallized volume fraction (crystallinity) formed during devitrification on the fracture toughness and offer a mechanistic model that can describe our, and previous, findings. For representative BMGs we consider $Zr_{44}Ti_{11}Cu_{10}Ni_{10}Be_{25}$ (Zr BMG) and $Pd_{43}Cu_{27}Ni_{10}P_{20}$ (Pd BMG) as BMGs with a low (Zr BMG) and high (Pd BMG) critical fictive temperature [20]. Crystallization is introduced through isothermal annealing. We found that up to 6% crystallinity does not measurably affect the BMG's fracture toughness. However, when the volume fraction reaches ~7%, a dramatic drop in fracture toughness K_Q occurs. We explain this dramatic behavior of K_Q utilizing finite element modeling by a rapid intensification of stresses in the amorphous matrix between two adjacent nanocrystal particles when a volume fraction of ~7% is approached.

Thermoplastic forming-based molding of BMG into silicon molds was utilized to fabricate the single-edge notched tensile (SENT) specimen samples (Fig. 1). Silicon molds were fabricated through photolithography and deep reactive ion etching (DRIE). Subsequently, these silicon molds were replicated with BMGs through TPF-based compression molding [Figs. 1(a)–1(b)]. To precisely control crystallized volume fraction, as-fabricated samples

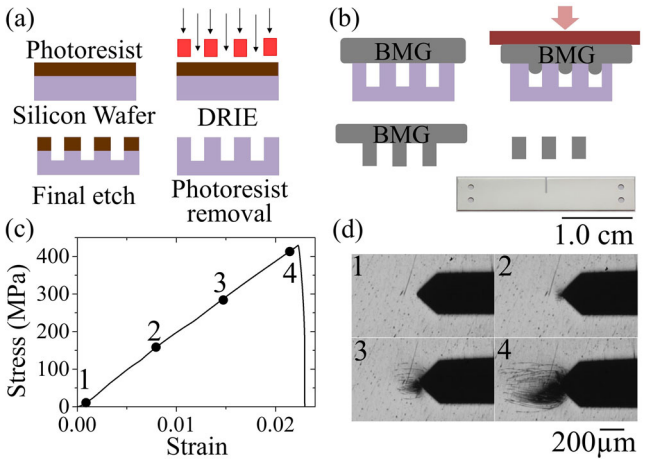

FIG. 1 (color online). BMG single edge notched tensile (SENT) fracture toughness fabrication technique comprises of (a) mold fabrication and (b) mold replication. (a) As-designed silicon mold fabricated by photolithography technique and deep reactive ion etching (DRIE) to accommodate SENT samples of $25 \times 5 \times 0.25$ mm^3 with a notch depth of 2.5 mm, $a/w = 0.5$, thickness of 250 ± 5 μm and a notch root radius of 10 μm. (b) Mold replication is achieved through thermoplastic forming based molding of the BMG into silicon mold at temperatures above T_g with application of pressure. (c) A typical stress-strain plot of Zr-BMG SENT, and (d) *in situ* observation of the development of the corresponding plastic zone.

 © 2015 American Physical Society

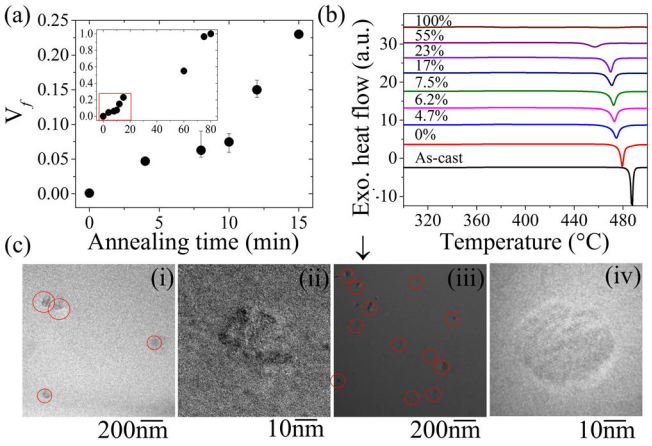

FIG. 2 (color online). Determination of the crystallized volume fraction through a combination of thermal analysis using differential scanning calorimetry (DSC) under a heating rate of 20 K/min (a),(b) and transmission electron microscopy (c). TEM bright field images of crystals embedded in the amorphous matrix of the sample with volume fraction of ~4% (i)–(ii), and ~7% (iii)–(iv).

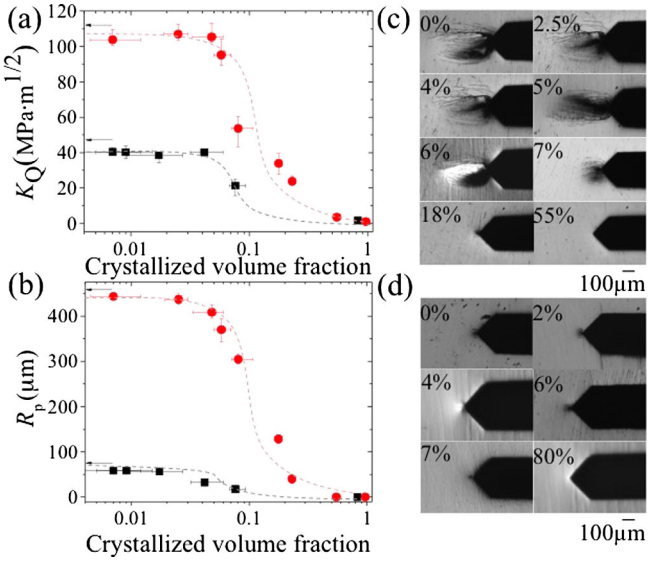

FIG. 3 (color online). (a) Measured K_Q as a function of the crystallized volume fraction for $Zr_{44}Ti_{11}Cu_{10}Ni_{10}Be_{25}$ (solid circle) and $Pd_{43}Cu_{27}Ni_{10}P_{20}$ (solid square). Errors originate from standard deviation from five samples per data point (vertical) and the evaluation of the crystallized volume fraction through thermal analysis and TEM (horizontal). The dashed lines help guide the eye. (b) Measured R_p for various degrees of crystallinity corresponding to each data point in (a). (c) *In situ* images of the critical plastic zone R_p, of Zr BMG prior to fracture. (d) *In situ* images of critical plastic zone of Pd BMG prior to fracture corresponding to (b).

were partially crystallized under isothermal annealing for various times in the supercooled liquid region in a heated liquid salt bath. In order to rule out thermal effects that can cause embrittlement of the glass phase, as has been reported previously [21–24], all samples were heated to $T_g + 10\,°C$ for 1 min to ensure the same thermal history for the glass phase in all samples. Crystallized volume fractions were quantified through thermal analysis upon subsequent heating with 20 K/ min quantified in the heat of crystallization [25]. In addition, transmission electron microscopy (TEM) was employed to alternatively determine size and crystallized volume fraction of crystals [Figs. 2(a)–2(c)]. Annealing times were chosen so as to result in crystallization of 0%, 2.5%, 4%, 5%, 6%, 7%, 18%, 55%, and 100% for Zr BMG and 0%, 2%, 4%, 6%, 7%, and 55% for Pd BMG. TEM reveals crystallized volume fractions (Fig. 2) with some discrepancy as compared to the volume fraction determined from DSC. This discrepancy is represented in the horizontal errors in Fig. 3(a).

Uniaxial tensile testing with quasistatic displacement control (initial strain rate of $10^{-4}\ s^{-1}$) was conducted to characterize the fracture toughness of the as-fabricated BMG SENT samples. The development of a plastic zone through shear band formation and propagation was captured by *in situ* microscopy during the deformation [Fig. 1(d)]. Because of the metastable nature of BMGs, which limits their size, it is generally difficult to obey standards to determine intrinsic plain strain toughness K_{IC}. Particularly for tough BMGs, K_Q is typically determined instead of K_{IC}. Following this strategy, the effect of crystallinity on fracture toughness of BMGs is quantified through the stress intensity factor $K_Q = \sigma\sqrt{\pi a}F(a/W)$, with a notch crack length (notch root radius $\rho = 10\ \mu m$, notch length $a = 2.5$ mm, sample width $W = 5$ mm, applied far-field stress σ, and sample configuration correction $F(a/W)$ [26], shown as $F(a/w) = \sqrt{(2W/\pi a)\tan(\pi a/2W)}\{0.752 + 2.02(a/w) + 0.37[1 - \sin(\pi a/2W)]^3\}/\cos(\pi a/2W))$. We measured the average K_Q of the as-fabricated Zr BMG sample to be ~103 MPa $m^{1/2}$. This number is comparable to the reported toughness of ~100 MPa $m^{1/2}$ for 7 mm thick $Zr_{41.2}Ti_{13.8}Cu_{12.5}Ni_{10.0}Be_{22.5}$ [27]. Most important for the presented study is the precise identification of relative changes; absolute values may have similar limitations as previous measurements on fracture toughness of BMGs.

The effect of crystallinity of Zr BMG on the fracture toughness is presented in Fig. 3(a). For a crystallinity of up to ~6%, no measurable effect was observed on K_Q. However, when crystallinity increases to ~7%, fracture toughness drops dramatically by ~50%. We observed a similar trend with a dramatic drop in K_Q ~7% crystallinity for Pd BMG [Fig. 3(a), black squares]. A further increase in crystallinity lowers the fracture toughness of both BMGs. For high crystallinity, K_Q approaches 1 MPa$\sqrt{m}$, which is close to the ideal brittle behavior for BMGs assuming a surface energy of 0.01 J/m^2 [28]. The observed decrease in the critical plastic zone R_p, shows a parallel trend to the fracture toughness dependence on crystallization [Fig. 3(b)].

Figures 3(c) and 3(d) shows plastic zone region of Zr-BMG and Pd-BMG, respectively.

Fracture toughness of BMGs has been associated with fracture surface roughness and fracture morphology [29–31]. To investigate a correlation between K_Q and surface roughness and morphology, we performed differential interface contrast (DIC) experiments to observe the overall surface roughness. We found that roughness on the fracture surface decreases as the crystal volume fraction increases (Fig. 4). (See Supplemental Material [32] for DIC analysis). Fully amorphous samples contain characteristic riverlike patterns, large veinlike patterns, and radiativelike patterns developed over the fracture surface. These features contribute to higher global surface roughness [30]. At ~6% crystallinity, the fracture morphology contains regions of river and radiativelike patterns with shallow and deep vein patterns coexisting. Such morphology has been previously associated with ductile behavior [36,37]. At 7% crystallinity, a high density of smaller vein patterns is present over the surface. The pattern suggests that the majority of the material remains amorphous, but the fracture surface appears more brittlelike, for example, as observed in the brittle Mg-based BMGs [1,31,38]. The observed trend of surface roughness and microstructures in the fractured surfaces agrees qualitatively with the correlation of fracture toughness and crystallinity.

In general, the mechanical properties of a composite such as a partially crystallized BMG forming alloy are determined by the properties of both the matrix and the secondary phase material (e.g., crystal), as well as their interface [39,40]. For example, the secondary phase can either increase or decrease the fracture toughness of a composite, which depends on the mechanical properties, volume fraction, size of the secondary phase, and interfacial strength between the matrix and the secondary phase [14,16,18,41–43]. In order to develop a mechanistic understanding of the effect of crystallinity on the fracture toughness of BMGs, we calculated the crystals' contribution to the strength of the composite. Previous studies revealed that strength directly scales with fracture toughness in Zr-based and Ni-based partially crystallized BMGs [44,45].

The strength of a particle-enhanced metal composite (σ_{CM}) can be quantified by the continuum shear lag model [46]

$$\sigma_{\mathrm{CM}} = \frac{1}{4} V_p \sigma_m s + V_m \sigma_m, \tag{1}$$

where σ_m is the yield stress of the matrix, V_p and V_m are the volume fraction of particles and matrix, respectively, and s is the particle size aspect ratio. Assuming a spherelike shaped crystalline phase, $s = 1$, and substituting $V_m = 1\text{-}V_p$, Eq. (1) becomes

$$\frac{\sigma_{\mathrm{CM}}}{\sigma_m} = \left(\frac{3}{4} - \frac{1}{2} V_p\right), \tag{2}$$

which suggests that the strength of composites linearly decreases as the crystal volume fraction increases. This relationship cannot rationalize the observed dramatic drop in K_Q at 7% crystallinity and considers neither the stress concentration nor interactions between the adjacent particles in the matrix.

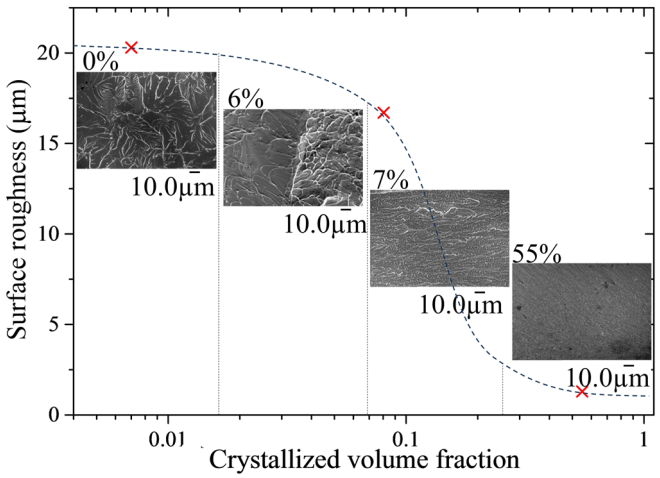

FIG. 4 (color online). Summary of the surface roughness on the fractured surface of Zr BMG with different crystallized volume fraction. Superimposed are scanning electron microscopy images of the fracture surfaces for amorphous, 6%, 7%, and 55% crystallinity. Roughness is measured from differential interface contrast (DIC) measurement, revealing a decrease in surface roughness with increasing crystallinity. Measured data are marked in red. The dashed line helps guide the eye.

We propose that such a sharp drop originates from the stress field interaction between particles. Even though crystals nucleate randomly during the very early stages of devitrification, due to the difference in composition between the liquid and the forming crystal, so called primary crystallization, which is typically present in metallic glass forming liquids, the distribution of the following crystals is controlled by the presence and location of previous crystals. Hence, the overall distribution of crystals during primary crystallization is more homogenous than a random distribution [47]. We simulate this scenario by a stress field interaction of two adjacent particles and observe the stresses at their center point, point B as shown in the inset of Fig. 5(a); see the Supplemental Material for simulation specifics [32].

The tensile stresses at point B ($\sigma_{yy,B}$) for different crystal fractions with the same far-field loading stress (1 GPa) and perfect interface are compared [dotted-red line in Fig. 5(a)]. An abrupt change in stress concentration is observed once the sample reaches ~7% crystallized volume fraction when we assume $G_{MG} < G_c$, $\sigma^f_{MG} > \sigma^f_c$, where G is the shear modulus and σ^f is the fracture strength, MG and c denote properties of the metallic glass and the crystals, respectively. In general, the shear modulus of the metallic glass is lower than the shear modulus of its competing crystal [35,48–51]. However, no clear trend has been observed for the fracture strength. In some cases the competing crystal's

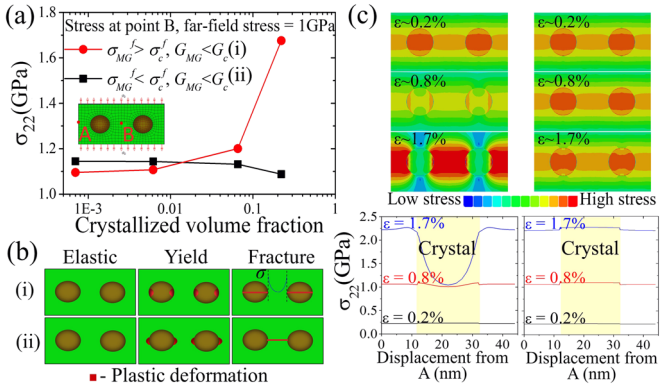

FIG. 5 (color online). Finite element analysis of the stress field interaction of crystals of various properties embedded in an amorphous matrix quantifying (a) stress in the matrix at the midpoint between two crystals (point B), reflecting the interaction between the crystals for $\sigma_{MG}^f < \sigma_c^f$, $G_{MG} < G_c$ (solid squares) and $\sigma_{MG}^f > \sigma_c^f$, $G_{MG} < G_c$ (solid circles) for various crystallized volume fractions (subscript MG denotes properties of the matrix, and c that of the crystals). The inset shows a unit cell containing two crystals under uniform tensile stress (σ_0) along the y direction used in the model setup. (b) The two possible cases for amorphous-nanocrystalline composites as a consequence of various properties of the crystals and amorphous matrix. Case (i) shows the progression of the system under tensile stress in (a), (red) solid circles. During elastic loading, the crystal carries larger stress than the amorphous matrix because $G_{MG} < G_c$. Further loading causes the crystal to fracture prior to the matrix as presented in our experiments. It is also possible that $\sigma_{MG}^f < \sigma_c^f$, $G_{MG} < G_c$ as in (a) [(black) solid squares] and is reflected in case (ii). Nanocrystal-BMG interfaces were considered in (c). The interfacial strength σ_i, between the metallic glass and the nanocrystals were varied in the simulation with its strength of $0.5\sigma_{MG}^f$ [(c), left] and $1.2\sigma_{MG}^f$ [(c), right]. For both cases in their elastic region, $\epsilon \sim 0.2\%$, the stress is higher in the crystal. With increasing far field stress resulting in a strain of $\epsilon \sim 1.7\%$, for weaker interface, $\sigma_i = 0.5\sigma_{MG}$ stress is highly concentrated in the amorphous matrix, whereas it is relatively uniformly distributed throughout the crystal, matrix, and interface for $\sigma_i = 1.2\sigma_{MG}^f$.

fracture strength has been found to be higher [3,14,52–54], and in others lower [35,44,48,51,55–58] than the fracture strength of the metallic glass. Therefore, we consider two cases here: (i) $G_{MG} < G_c$, $\sigma_{MG}^f > \sigma_c^f$ and (ii) $G_{MG} < G_c$, $\sigma_{MG}^f < \sigma_c^f$. For case (i) [Fig. 5(b)i], upon elastic loading, the stresses in the crystals are higher than in the matrix due to the larger shear modulus of the crystals. This causes fracture to first occur in the crystal phase. Such fracture creates sharp rises in stress, which can drastically increase stresses in the matrix. This enhancement of stresses in the matrix becomes effective once crystallization volume fraction exceeds ~7% [Fig. 5(a)]. As a result, metallic glasses including more than ~7% crystallinity with $G_{MG} < G_c$, $\sigma_{MG}^f > \sigma_c^f$ embrittles. Such a behavior is most typical for partially crystallized BMGs. In case (ii), $\sigma_{MG}^f < \sigma_c^f$, $G_{MG} < G_c$, the secondary phase carries higher load than the matrix, and stresses are therefore reduced in the matrix for the same far-field stress [Fig. 5(a)-black line, and Figs. 5(b)ii]. This causes delayed shear band formation before eventual fracture and, hence, increased toughness. Such a behavior, even less common, may have been observed in some previous studies [3,53].

So far, the discussed cases assumed a perfect interface. However, if σ_i has a final strength comparable to the strength of σ_{MG} or σ_c, embrittlement can also occur even if $\sigma_{MG}^f < \sigma_c^f$ and $G_{MG} < G_c$ [Fig. 5(c)]. The reason for this is that a damaged interface generates stress concentrations in the amorphous matrix similar to a fractured crystal and, as a result, embrittles the material. Therefore, in order to observe a toughening behavior in a partially crystallized BMG, $\sigma_{MG}^f < \sigma_c^f$ and $G_{MG} < G_c$ must hold true, and the interface between the two phases must be strong such that fracture does not originate from the interface. Figure 5(c) compares simulation results for variations of σ_i of $0.5\sigma_{MG}$ and σ_i of $1.2\sigma_{MG}$ for the case of $\sigma_{MG}^f < \sigma_c^f$ and $G_{MG} < G_c$. At $\epsilon \sim 0.2\%$, stress is higher in the crystal phase. At $\epsilon \sim 0.8\%$ of the system with $\sigma_i = 0.5\sigma_{MG}$, stresses migrate from the crystal to the interface and induce high stress concentration on the amorphous matrix ($\epsilon \sim 1.7\%$), while this behavior is not observed in systems with $\sigma_i = 1.2\sigma_{MG}$ due to the fracturing of the interface for $\sigma_i = 0.5\sigma_{MG}$ compared to the still intact interface for $\sigma_i = 1.2\sigma_{MG}$.

It is important to mention that the above cases do not represent previously observed toughening in BMG composites where the secondary phases are large in size and spacing [41,59,60]. For these composites, the secondary phase is spaced such that it coincides with the plastic zone size of the matrix. The softer secondary crystalline phases reduce stress through absorbing strain, and hence shear band formation without fracture. These plastic zone sizes are on the order of ~100 microns, which is about 10 000 times larger than the spacing of the secondary phase in our present case.

The complete mechanical behavior of composites is more complicated than discussed here, but we propose that their behavior and interactions can be categorized into two scenarios, one of which reflects our experimental findings. For $\sigma_{MG}^f < \sigma_c^f$ and $G_{MG} < G_c$, crystallization can enhance toughness. Typically, and experimentally observed here, $\sigma_{MG}^f > \sigma_c^f$ and $G_{MG} < G_c$ and the deformation of the nanocrystals induces a high stress concentration in the BMG. Therefore, failure occurs at low deformation, which is indicative of embrittlement. For both cases, the transition region was observed around 7% crystallization by volume.

In conclusion, we have observed a highly nonlinear dependence of crystallinity of BMG forming alloys on their fracture toughness. Below ~6%, crystallinity does not appear to affect their fracture toughness. This finding is

very encouraging for thermoplastic forming processing of BMGs where, even though highly predictable, small amounts of crystallinity are unavoidable. A dramatic drop occurs above ~7% where minute additional crystallinity drastically degrades fracture resistance. This behavior can be explained by the stress field interaction of the typically stiffer but lower fracture strength crystalline inclusion.

This work was supported by the Department of Energy through the Office of Basic Energy Sciences (No. DE SC0004889). The authors would like to thank Michael Power and William Salema for their assistance in sample preparation.

*Corresponding author.
ze.liu@whu.edu.cn
†Corresponding author.
jan.schroers@yale.edu

[1] X. Xi, D. Zhao, M. Pan, W. Wang, Y. Wu, and J. Lewandowski, Phys. Rev. Lett. **94**, 125510 (2005).
[2] J. Schroers and W. Johnson, Phys. Rev. Lett., **93**, 255506 (2004).
[3] J. Das, M. Tang, K. Kim, R. Theissmann, F. Baier, W. Wang, and J. Eckert, Phys. Rev. Lett. **94**, 205501 (2005).
[4] C. P. Kim, J.-Y. Suh, A. Wiest, M. L. Lind, R. D. Conner, and W. L. Johnson, Scr. Mater. **60**, 80 (2009).
[5] M. D. Demetriou, M. E. Launey, G. Garrett, J. P. Schramm, D. C. Hofmann, W. L. Johnson, and R. O. Ritchie, Nat. Mater. **10**, 123 (2011).
[6] J. Xu, U. Ramamurty, and E. Ma, JOM **62**, 10 (2010).
[7] J. J. Lewandowski, Mater. Trans., JIM **42**, 633 (2001).
[8] W. L. Johnson, MRS Bull. **24**, 42 (1999).
[9] J. Schroers, Adv. Mater. **22**, 1566 (2010).
[10] Y. T. Shen, L. Q. Xing, and K. F. Kelton, Philos. Mag. **85**, 3673 (2005).
[11] K. F. Kelton, T. K. Croat, A. K. Gangopadhyay, L. Q. Xing, A. L. Greer, M. Weyland, X. Li, and K. Rajan, J. Non-Cryst. Solids **317**, 71 (2003).
[12] C. J. Gilbert, R. O. Ritchie, and W. L. Johnson, Appl. Phys. Lett. **71**, 476 (1997).
[13] M. Song, Y.-q. Li, Z.-g. Wu, and Y.-h. He, J. Non-Cryst. Solids **357**, 1239 (2011).
[14] A. C. Lund and C. A. Schuh, Philos. Mag. Lett. **87**, 603 (2007).
[15] C. Fan, C. Li, A. Inoue, and V. Haas, Phys. Rev. B **61**, R3761 (2000).
[16] R. Raghavan, V. V. Shastry, A. Kumar, T. Jayakumar, and U. Ramamurty, Intermetallics **17**, 835 (2009).
[17] N. Nagendra, U. Ramamurty, T. T. Goh, and Y. Li, Acta Mater. **48**, 2603 (2000).
[18] C. Fan, C. Li, A. Inoue, and V. Haas, Phys. Rev. B **61**, R3761 (2000).
[19] A. Inoue, W. Zhang, T. Tsurui, A. R. Yavari, and A. L. Greer, Philos. Mag. Lett. **85**, 221 (2005).
[20] G. Kumar, P. Neibecker, L. Yanhui, and J. Schroers, Nat. Commun. **4**, 1536 (2013).
[21] W. Li, H. Bei, Y. Tong, W. Dmowski, and Y. F. Gao, Appl. Phys. Lett. **103**, 171910 (2013).
[22] Y. Fan, T. Iwashita, and T. Egami, Phys. Rev. Lett.**115**, 045501 (2015).
[23] Z. Evenson, B. Ruta, S. Hechler, M. Stolpe, E. Pineda, I. Gallino, and R. Busch, Phys. Rev. Lett. **115**, 175701 (2015).
[24] G. Kumar, D. Rector, R. D. Conner, and J. Schroers, Acta Mater. **57**, 3572 (2009).
[25] L. C. Chen and F. Spaepen, J. Appl. Phys. **69**, 679 (1991).
[26] H. Tada, P. C. Paris, and G. R. Irwin, *The Stress Analysis of Cracks Handbook*, 3rd ed (ASME Press, New York, 2000).
[27] P. Lowhaphandu and J. J. Lewandowski, Scr. Mater. **38**, 1811 (1998).
[28] J. J. Lewandowski, W. H. Wang, and A. L. Greer, Philos. Mag. Lett. **85**, 77 (2005).
[29] J.-Y. Suh, R. Dale Conner, C. Paul Kim, M. D. Demetriou, and W. L. Johnson, J. Mater. Res. **25**, 982 (2010).
[30] A. Tatschl, C. J. Gilbert, V. Schroeder, R. Pippan, and R. O. Ritchie, J. Mater. Res. **15**, 898 (2000).
[31] G. Wang, D. Zhao, H. Bai, M. Pan, A. Xia, B. Han, X. Xi, Y. Wu, and W. Wang, Phys. Rev. Lett. **98**, 235501 (2007).
[32] See Supplemental Material http://link.aps.org/supplemental/10.1103/PhysRevLett.115.265502 for additional information on material preparation, sample characterization, and detailed parameters used in simulation, along with additional simulation results from finite element analysis, which includes Refs. [33–35].
[33] P. A. Gustafson and A. M. Waas, Int. J. Solids Struct. **46**, 2201 (2009).
[34] S. Li, M. D. Thouless, A. M. Waas, J. A. Schroeder, and P. D. Zavattieri, Compos. Sci. Technol. **65**, 281 (2005).
[35] D. Okai, M. Inoue, T. Mori, T. Fukami, T. Yamasaki, H. M. Kimura, and A. Inoue, J. Alloys Compd. **504**, S95 (2010).
[36] F. Spaepen, Acta Metall. **23**, 615 (1975).
[37] C. J. Gilbert, V. Schroeder, and R. O. Ritchie, Metall. Mater. Trans. A **30**, 1739 (1999).
[38] R. Raghavan, P. Murali, and U. Ramamurty, Intermetallics **14**, 1051 (2006).
[39] W. H. Wang, Prog. Mater. Sci. **52**, 540 (2007).
[40] C. Schuh, T. Hufnagel, and U. Ramamurty, Acta Mater. **55**, 4067 (2007).
[41] D. C. Hofmann, J. Y. Suh, A. Wiest, G. Duan, M. L. Lind, M. D. Demetriou, and W. L. Johnson, Nature (London) **451**, 1085 (2008).
[42] F. Szuecs, C. P. Kim, and W. L. Johnson, Acta Mater. **49**, 1507 (2001).
[43] A. V. Sergueeva, N. Mara, and A. K. Mukherjee, J. Non-Cryst. Solids **317**, 169 (2003).
[44] S. Qiu, K. Yao, and P. Gong, Sci. China Phys. Mech. Astron. **53**, 424 (2010).
[45] D. G. Ast and D. Krenitsky, Mater. Sci. Eng. **23**, 241 (1976).
[46] D. J. Lloyd, Int. Mater. Rev. **39**, 1 (1994).
[47] K. F. Kelton, Philos. Mag. Lett. **77**, 337 (1998).
[48] G. E. Abrosimova, N. S. Afonikova, N. P. Kobelev, E. L. Kolyvanov, and V. A. Khonik, Phys. Solid State **49**, 2099 (2007).
[49] G. E. Abrosimova, N. P. Kobelev, E. L. Kolyvanov, and V. A. Khonik, Phys. Solid State **46**, 1859 (2004).
[50] N. P. Kobelev, V. A. Khonik, G. V. Afonin, and E. L. Kolyvanov, J. Non-Cryst. Solids **411**, 1 (2015).

[51] W. H. Wang, R. J. Wang, G. J. Fan, and J. Eckert, Mater. Trans., JIM **42**, 587 (2001).
[52] G. Y. Wang, P. K. Liaw, Y. Yokoyama, M. Freels, R. A. Buchanan, A. Inoue, and C. R. Brooks, J. Mater. Res. **22**, 493 (2007).
[53] Y. C. Kim, J. H. Na, J. M. Park, D. H. Kim, J. K. Lee, and W. T. Kim, Appl. Phys. Lett. **83**, 3093 (2003).
[54] G. Wang, J. Shen, Q. H. Qin, J. F. Sun, Z. H. Stachurski, and B. D. Zhou, J. Mater. Sci. **40**, 4561 (2005).
[55] D. J. Safarik and R. B. Schwarz, Acta Mater. **55**, 5736 (2007).
[56] J. Fornell, S. González, E. Rossinyol, S. Suriñach, M. D. Baró, D. V. Louzguine-Luzgin, J. H. Perepezko, J. Sort, and A. Inoue, Acta Mater. **58**, 6256 (2010).
[57] B. Zhang, R. J. Wang, and W. H. Wang, Phys. Rev. B **72**, 104205 (2005).
[58] L. Charleux, S. Gravier, M. Verdier, M. Fivel, and J. J. Blandin, J. Mater. Res. **22**, 525 (2007).
[59] B. Sarac and J. Schroers, Nat. Commun. **4**, 2158 (2013).
[60] C. Fan, R. T. Ott, and T. C. Hufnagel, Appl. Phys. Lett. **81**, 1020 (2002).